Brazilian Journal of Physics (2024) 54:35
https://doi.org/10.1007/s13538-023-01415-5

GENERAL AND APPLIED PHYSICS

Biological Activities of Boron and Reduced Graphene Oxide-Based Zinc Oxide Nanocomposites (ZnO:B and RGO/ZnO:B) Synthesized by an Environmentally Friendly Method

Saniye Tekerek[1,2] · **Ayça Tanrıverdi**[1,2] · **Esin Kiray**[3] · **Esen Çakmak**[4,5]

Received: 6 October 2023 / Accepted: 20 December 2023 / Published online: 28 December 2023

Abstract
In this study, a graphene oxide material was fabricated using the Hummers process. RGO, ZnO, ZnO:B and RGO/ZnO:B nanoparticles were synthesized by the hydrothermal method in an autoclave at a temperature of 160 °C. The structural and morphological changes in the synthesized ZnO nanomaterials were investigated by preparing composite materials with a boron additive and RGO. The prepared nanoparticles were characterized by X-ray diffraction (XRD) and scanning electron microscopy (SEM). Antimicrobial and antibiofilm assays were performed to evaluate the biological activities of the synthesized nanoparticles. The antimicrobial activity of these NPs was investigated against *Escherichia coli*, *Pseudomonas aeruginosa*, *Staphylococcus aureus*, *Bacillus cereus*, *Enterococcus faecalis* and *Staphylococcus epidermidis* pathogenic bacteria. Among the nanoparticles tested, ZnO and ZnO:B NPs showed strong antimicrobial activity against clinically important *E. coli*, *P. aeruginosa* and *B. cereus strains*. The antibiofilm activity of the synthesized nanoparticles was determined using *E. coli* and *P. aeruginosa* strains. The biofilm inhibition of both strains by the ZnO:B nanocomposites was greater than that by the other nanocomposites. At a concentration of 20 mg/mL, the ZnO:B nanocomposite showed 42.13% biofilm inhibition of *E. coli* and 36.21% biofilm inhibition of *P. aeruginosa*. The RGO/ZnO:B nanocomposite had a specific inhibitory effect on *E. coli* (34.25%) and *P. aeruginosa* (30.16%). The antibiofilm effect of the nanocompounds used in the study was greater on *E. coli* than on *P. aeruginosa*. As a result, the synthesized boron-reinforced ZnO nanocomposites exhibited strong biological effects. These results will provide valuable information for the development of new treatment regimens for the inactivation of pathogenic bacteria.

Keywords Nanocomposite · Boron · ZnO · Antimicrobial · Antibiofilm

✉ Saniye Tekerek
saniye1580@gmail.com

1 Dept. of Opticianry, Vocational School of Health Services, Kahramanmaraş Sutcu Imam University, Kahramanmaras, Turkey

2 Department of Material Science and Engineering, Graduate School of Natural and Applied Sciences, Kahramanmaras Sutcu Imam University, Kahramanmaras, Turkey

3 Department of Medical Services and Techniques, Medical Laboratory Techniques Program, Ahi Evran University, Vocational School of Health Services, Kırşehir, Turkey

4 Dept. of Medical Services and Techniques, Vocational School of Health Services, Kahramanmaras Sutcu Imam University, Kahramanmaras, Turkey

5 Department of Bioengineering and Sciences, Graduate School of Natural and Applied Sciences, Kahramanmaraş Sutcu Imam University, Kahramanmaras, Turkey

1 Introduction

The emergence of antibiotic-resistant pathogens has become a serious health problem. Resistance to antibiotics in infections caused by microorganisms is one of the most important factors that increase morbidity and mortality in infected individuals [1]. Bacteria can be naturally resistant to certain antibiotics, but they can also develop resistance to antibiotics through genetic mutations [2]. Moreover, incorrect use and excessive use of antibiotics has led to the emergence of resistant bacteria [3, 4]. Biofilms produced by most pathogenic bacteria contribute to the development of resistance, reducing or neutralizing the effect of antimicrobial agents [5]. Antibiotics are common treatment methods for bacterial infections. The dramatic increase in bacterial resistance to antibiotics now threatens the success of treatment. Therefore, new antimicrobial agents are

needed as alternatives to traditional antibiotics for treating antibiotic-resistant bacterial infections.

Nanotechnology addresses the production, application and characterization of materials at the nanoscale. Recently, nanotechnology has been widely researched in various fields of science, such as chemistry, materials science, physics and biotechnology [6]. Biocompatible nanoparticles are also widely used in biomedical applications due to their unique physical and chemical properties [7, 8]. The most attractive feature of nanoparticles (NPs) is the increase in the surface-to-volume ratio because their size decreases to the nanoscale [9]. Today, many methods are used in the production of nanoparticles and their derivatives. Among these methods, hydrothermal synthesis is the most widely used method because it is inexpensive, has uncomplicated experimental processes, involves the production of homogeneous and pure materials, and is an environmentally friendly method [10, 11].

Many studies have demonstrated that various nanoparticles and their derivatives have potential effects on biological applications, such as antimicrobial, anticancer and antibiofilm properties [12–14]. Zinc oxide nanoparticles (ZnO NPs) are among the most popular nanoparticles used in antimicrobial applications. The most important advantages of ZnO NPs include that they are environmentally friendly, easy to prepare, nontoxic, biosafe and biocompatible. Because of their exceptional antibacterial and antibiofilm properties, it is believed that ZnO NPs may serve as an alternative in biomedical applications [7]. Recently, new nanocomposites based on metal oxides have been synthesized with the addition of materials such as graphene, boron and chitosan, and their synergistic effects have been investigated in biological applications [15, 16]. In addition, new composites are created by adding materials such as graphene and chitosan to nanoparticles, and new microbial agents are being discovered [17, 18]. Previous studies have reported that graphene-based materials (such as graphene, graphene oxide (GO) and reduced GO (RGO)) exhibit strong antimicrobial activities when conjugated with nanoparticles [12]. In studies on boron, the antimicrobial activities of boron-containing nanomaterials, nanosheets and boron-doped nanoparticles have been investigated, and it has been determined that boron has strong therapeutic potential [15, 16, 19, 20]. However, the role of this compound in NP synthesis and biological applications has still not been clarified, and related research has remained quite limited.

Among composite materials, graphene sheets decorated with metal oxide nanoparticles exhibit exceptional properties due to synergistic interactions [21]. Biological applications of ZnO-metal oxide composites such as ZnO/Ag [22], ZnO/RGO [23], ZnO/CuO [24], ZnO/TiO [25], and ZnO/TiO2 [25] have been reported in the literature. Previous studies have reported that RGO and ZnO have antimicrobial activity when conjugated with active ingredients [12]. Because of the properties of ZnO, RGO and boron, the effects of the synergistic effects of ZnO:B (two-component) and RGO/ZnO:B (three-component) nanocomposites on biological activities were investigated in this article.

In this study, ZnO and RGO nanoparticles were synthesized by a hydrothermal method, which is an environmentally friendly method. By preparing two-component (ZnO:B) and three-component (RGO/ZnO:B) nanocomposites from the synthesized nanoparticles, the structural and morphological changes were investigated. These nanocomposites were characterized by SEM and XRD, and their antimicrobial and antibiofilm properties were determined. Biological activity studies of ZnO and RGO nanoparticles and their composites are available in the literature. However, only a limited number of studies on the application of two- and three-nanocomponent biological activity, especially with boron additives, exist. The aim of this study was to determine the potential of two-component (ZnO:B) and three-component (RGO/ZnO:B) nanocomposites as alternative microbial agents to antibiotics.

2 Materials and Methods

2.1 Materials for the Experimental Process

The materials used were graphite powder (< 20 µm, synthetic) from Aldrich, sulfuric acid (H_2SO_4, 95–97%, Merck), potassium permanganate ($KMnO_4$, extra pure, Tekkim), hydrogen peroxide (H_2O_2, 35%, Merck), hydrochloric acid (HCl, ≥ 37%, Sigma Aldrich), zinc nitrate hexahydrate ($Zn(NO_3)_2.6H_2O$, 98%, Sigma Aldrich), hexamethylene tetramine ($C_6H_{12}N_4$, HMT, Merck), boric acid (H_3BO_3, 98.5%), ammonia solution (25%, Merck), potassium hydroxide (KOH, 90% Tekkim), and ethanol (C_2H_5OH, Isolab Chemicals).

2.2 Graphene Oxide (GO) Synthesis

The synthesis of graphene oxide (GO) was carried out in 3 stages, namely, at low temperature, medium temperature and high temperature, according to the methods of Hummers. Step 1 (low temp. Briefly, 2 g of graphite powder was added to sulfuric acid (H_2SO_4), the temperature of which was maintained at approximately 3 °C, and the mixture was placed in an ice bath on a magnetic stirrer. The solution was stirred for 30 min to obtain a dense, grayish liquid. Then, 8 g of potassium permanganate ($KMnO_4$) was slowly added to the mixture. Care was taken to ensure that the solution did not exceed 10 °C when added. The color of the solution changed to dark green. Stirring was continued for 2 h in an ice bath. In step 2 (medium temp.), the solution was placed in a water

bath at 35 °C and stirred for 1 h. One hundred milliliters of ultrapure water was added to the concentrated solution. The concentrated solution was slowly diluted with 100 mL of ultrapure water. After adding pure water, the solution color became brown, and the solution temperature was measured at 35 °C. In step 3 (high temp.), the solution was placed in a preprepared water bath at 95 °C for 15 min. When the solution temperature reached 95 °C, the solution was diluted again with 300 mL of high-purity water. The color of the solution changed to yellow. By the addition of 20 mL of 35% hydrogen peroxide (H_2O_2) to the mixture, the $KMnO_4$ was completely reduced. Bubbles were observed emerging from the solution, and the solution color turned bright yellow. The solution was left for 24 h, after which the precipitate was observed. The resulting precipitate was washed with 800 mL of aqueous solution containing 5% hydrochloric acid (HCl). The metal ions in the precipitate were removed. The filtered mixture was washed with 1 L of ultrapure water to remove acid. The resulting brown precipitate was dried at room temperature, and GO was obtained. Figure 1 shows a schematic view of the production processes and experimental mechanisms of GO material.

2.3 Reduced Graphene Oxide (RGO) Synthesis

The production of RGO (reduced graphene oxide) was carried out by the hydrothermal method. 0.1 g of GO was mixed with 20 mL of pure water and 10 mL of ethanol. The mixture was kept in an ultrasonic bath for 3 h. This solution was put into a Teflon-lined autoclave. The mixture was kept in an autoclave muffle furnace at 160 °C for 3 h. The RGO nanoparticles were filtered and dried at room temperature.

2.4 Preparation of ZnO and ZnO:B Nanoparticles

Hydrothermal synthesis was used to prepare zinc oxide (ZnO) and boron-doped zinc oxide (ZnO:B) nanoparticles. Zinc nitrate (0.1 M; $Zn(NO_3)_2.6H_2O$) and 0.1 M hexamethylenetetramine ($C_6H_{12}N_4$) salts were dissolved separately in 50 mL of pure water and mixed with a magnetic stirrer for 30 min. The solutions were mixed. Ammonia was added dropwise. The pH of the solution was adjusted to 9. Next, the solution was placed in a Teflon-lined autoclave at 160 °C in a muffle furnace for 3 h. The formed ZnO nanoparticles were filtered and washed 3 times with pure water for removal of organic compounds. ZnO:B

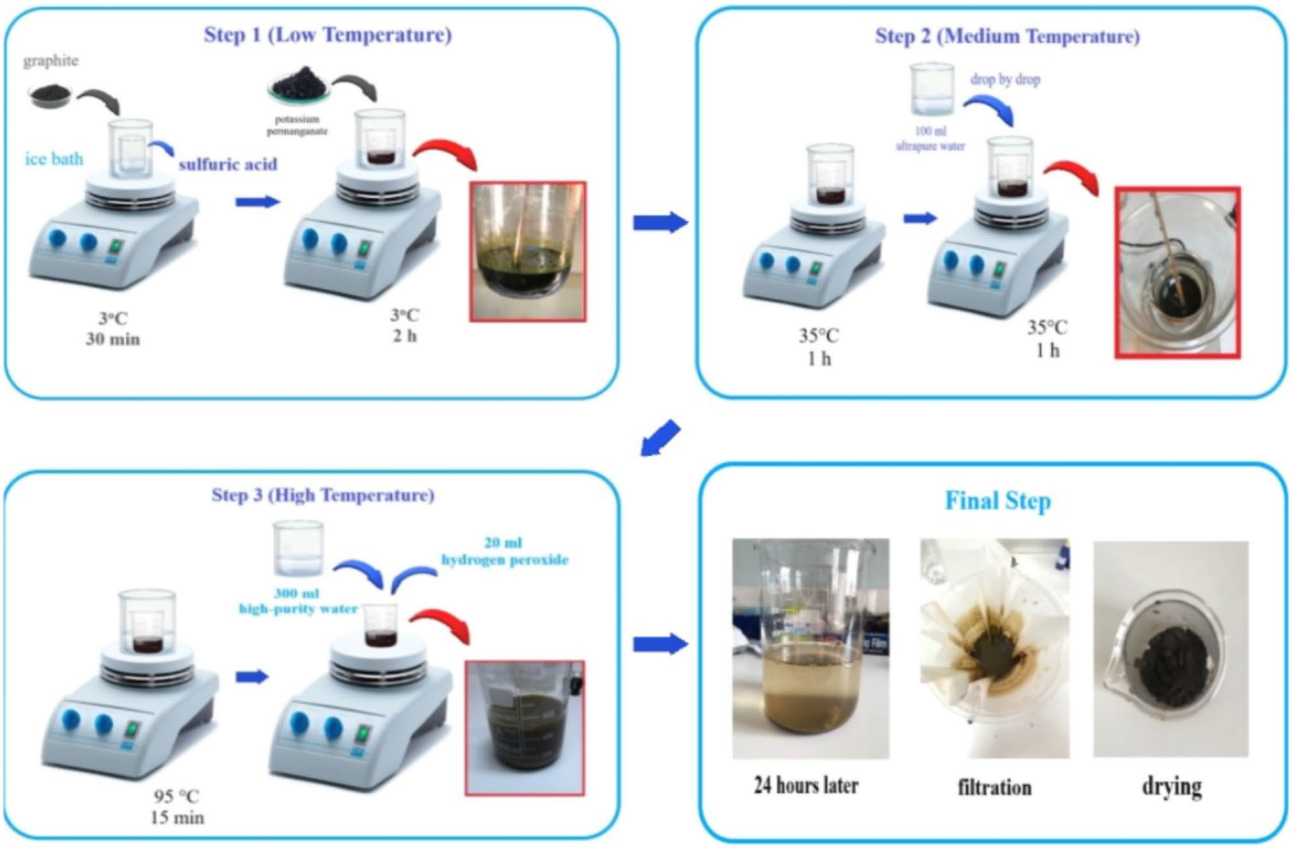

Fig. 1 Synthesis Stages of GO Materials Made by the Hummers Process

nanoparticles were prepared by the same experimental process. Zinc nitrate (0.1 M; $Zn(NO_3)_2.6H_2O$), 0.1 M hexamethylene tetramine ($C_6H_{12}N_4$) and 5% by weight 0.1 M boric acid (H_3BO_3) were dissolved in a total of 100 mL of pure water and mixed with a magnetic stirrer for 30 min. The solution pH was adjusted to 9 with ammonia. The solution was placed in a Teflon-lined autoclave and kept in a muffle furnace at 160 °C for 3 h. ZnO:B nanoparticles were filtered. The samples were washed 3 times with pure water. The obtained ZnO and ZnO:B nanoparticles were annealed at 450 °C for 1 h to characterize them.

2.5 RGO/ZnO:B Nanocomposite Synthesis

RGO/ZnO:B composite particles were prepared by a hydrothermal process. Pure water (20 mL) and 10 mL of ethanol (C_2H_5OH) were added to 0.1 g of GO, which was synthesized according to the Hummers' method. The solution was kept in an ultrasonic bath for 1 h. First, 0.1 g of synthesized ZnO:B nanoparticles was added to the solution. Subsequently, the solution was placed in an ultrasonic bath for 2 h. The resulting suspension was then placed in a Teflon-lined autoclave. The autoclave was kept at 160 °C for 3 h. In this way, graphene oxide was converted to reduced graphene oxide, and a chemically bonded RGO/ZnO:B composite material was obtained. A Philips X'Pert PRO, Perkin Elmer 400 FT-IR spectrometer, Shimadzu UV-1800 and Zeiss EVO 10LS instruments were used for characterization. The analyses were carried out in the laboratory of the Kahramanmaras Sutcu Imam University USKIM (University Industry State Cooperation Center).

2.6 Antimicrobial Activity

The antimicrobial activity of the synthesized nanoparticles was evaluated by the agar well diffusion method. *Escherichia coli* ATCC 25922, *Pseudomonas aeruginosa* ATCC 27853, *Staphylococcus aureus* ATCC 25923, *Bacillus cereus* ATCC 14579, *Enterococcus faecalis* ATCC 29212 and *Staphylococcus epidermidis* ATCC 12228 were used in the antimicrobial analysis. One hundred microliters of overnight activated cultures were inoculated onto agar plates, and 100 µl of NPs (at a concentration of 100 mg/mL) was subsequently added by opening the wells on the plates. The plates were then incubated for 24 h at 37 °C. Antimicrobial activity was determined by measuring the inhibition zone diameter (mm). This study was performed in three replicates [26].

2.7 Minimum Inhibitory Concentration (MIC) Determination

The minimal inhibitory concentration (MIC) was determined using a modified standard of the Clinical and Laboratory Standards Institute (CLSI) liquid microdilution method. *Escherichia coli* ATCC 25922, *Pseudomonas aeruginosa* ATCC 27853, *Staphylococcus aureus* ATCC 25923, *Bacillus cereus* ATCC 14579, *Enterococcus faecalis* ATCC 29212 and *Staphylococcus epidermidis* ATCC 12228 type strains were used in the study. MIC determination was performed in 96-well plates using TSB medium. The cultures were incubated overnight at 37 °C and diluted to 1×10^6 CFU/mL, after which 50 µl of bacteria was inoculated into each well. The samples were added to 96-well plates at a volume of 50 µL and at different concentrations (256–0.5 µM) and incubated at 37 °C for 18 h. The minimum concentration without visible bacterial growth was defined as the MIC. Gentamicin (Sigma Aldrich, USA) was used as a positive control [27].

2.8 Antibiofilm Activity

Biofilm-producing *E. coli* ATCC 25922 and *P. aeruginosa* ATCC 27853 type strains were used to determine the antibiofilm activity of the synthesized NPs. After serial dilutions, 100 mL of sample (1.25–20 mg/mL) and 100 mL of bacterial culture (OD600 = 0.132) activated in TSB medium at 37 °C were transferred to 96-well plates. After 24 h of incubation at 37 °C, the cells adhering to the wells were carefully rinsed with distilled water and allowed to air dry. Staining was performed with 0.4% (w/v) crystal violet in an aseptic environment, followed by rinsing with pure water. Crystal violet was dissolved in 200 mL of ethanol. TSB medium (100 mL) was used as a negative control, and sample-free bacterial cultures were used as a positive control. The absorbance of the wells was measured at 595 nm (BioTek Epoch 2 Microplate Spectrophotometer). The antibiofilm activity (%) was determined by the formula below [28]. The study was repeated three times.

$$\text{Antibiofilm activity}\,(\%) = (1 - \text{OD sample}/\text{OD control}) \times 100$$

3 Results and Discussion

3.1 Characterization

3.1.1 Graphene Oxide (GO) Characterization

GO was prepared by the Hummers method and characterized by X-ray diffraction (XRD), Fourier transform infrared spectroscopy (FTIR), scanning electron microscopy (SEM) and UV−Vis spectroscopy (UV). [29]. The XRD pattern of the synthesized GO is given in Fig. 2(a). The (001) peak of GO is observed at $2\theta = 11.24°$, as shown in Fig. 2(a). As a result of XRD analysis, the distance d between the (001) planes was measured to be 0.78 nm [30]. These results are smaller than the interplanar distance of natural graphite

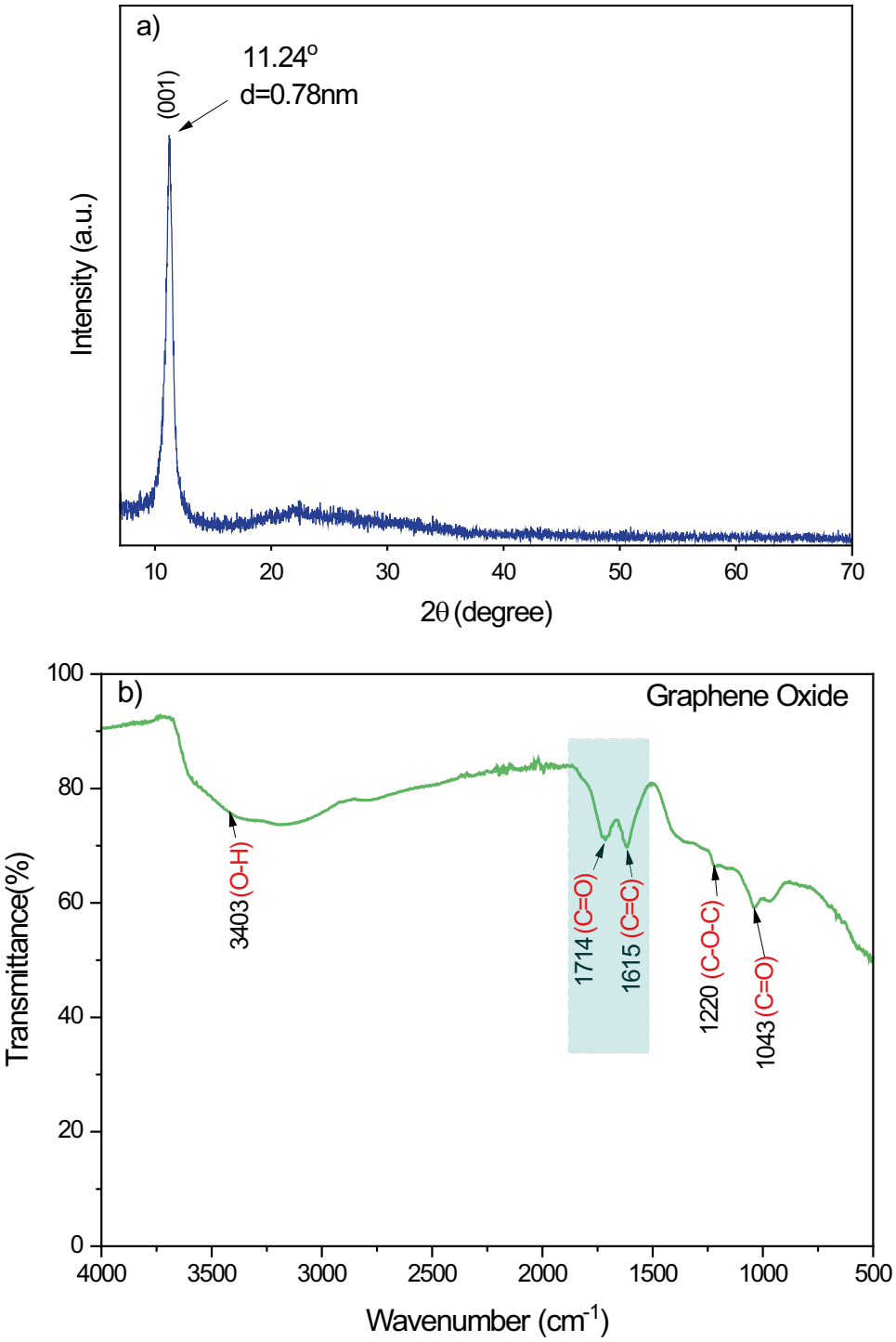

Fig. 2 **a** XRD pattern of GO and **b** FTIR spectrum of GO

(d = 0.34 nm). This indicates that oxygenated functional groups (hydroxyl, carbonyl, carboxyl, epoxy, etc.) penetrate between graphite planes, causing structural defects and converting natural graphite to GO [31]. Among these functional groups, epoxy and hydroxyl groups were scattered inside the 2D GO plane, while carbonyl and carboxyl groups were localized at the edges of the GO plane.

The FTIR spectrum of the prepared GO is shown in Fig. 2(b). The spectra show that GO contains oxygen-containing functional groups [32]. In the FTIR spectrum, 3403 cm^{-1} corresponds to hydroxyl groups (-OH), 1714 cm^{-1} to carboxyl groups (-C = O), 1615 cm^{-1} to C = C, 1220 cm^{-1} to epoxy groups (-C–O–C) and 1043 cm^{-1} to C-O groups (-C-O) [33].

An electron microscopy (SEM) image of GO is presented in Fig. 3 (a). As shown in Fig. 3a, two-dimensional GO layers are folded into planes [34]. These folds are formed by the oxygen-containing functional groups that appear during the formation of GO and the structural defects that result from them [33]. Figure 3(b) shows the UV absorbance spectrum of the produced GO. A peak corresponding to the $\pi \rightarrow \pi^*$ transition between C–C bonds is observed at 233 nm. The shoulder peak observed at 300 nm corresponds to the $\pi \rightarrow \pi^*$ transition between the aromatic C–C bonds.

3.1.2 Characterization of the RGO, ZnO, ZnO:B and RGO/ZnO:B Nanoparticles

XRD patterns of the (a) RGO, (b) ZnO, (c) ZnO:B and (d) RGO/ZnO:B nanoparticles are shown in Fig. 4. When the XRD pattern was examined, two peaks were observed at 25° and 43°, which belong to the RGO that was reduced

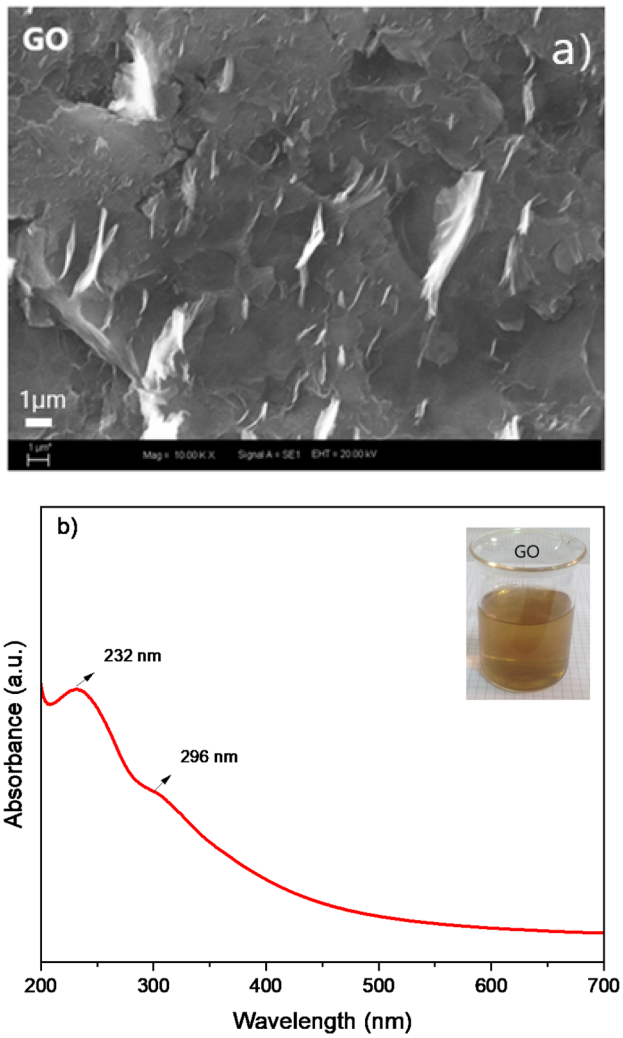

Fig. 3 **a** SEM image of GO and **b**UV spectrum of GO

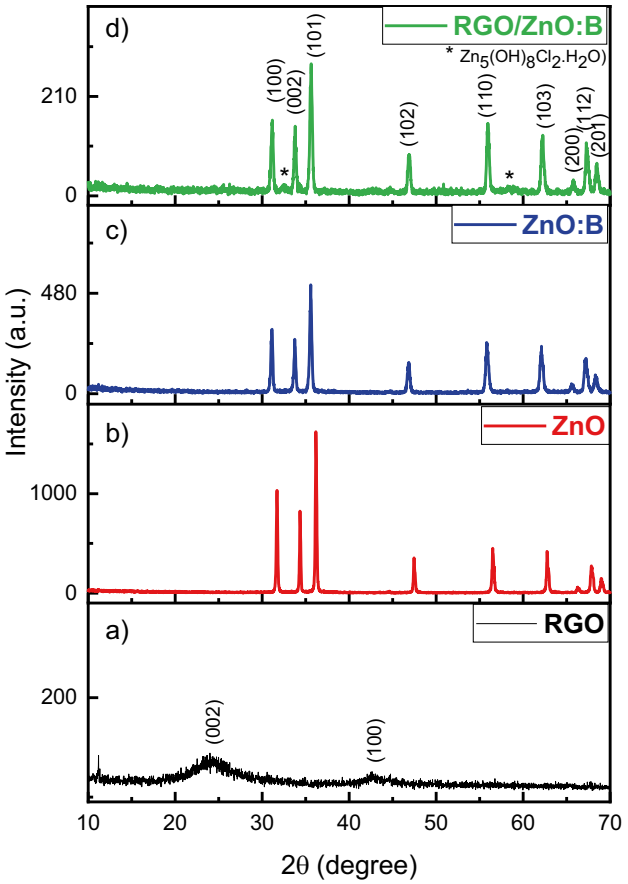

Fig. 4 XRD patterns of **a** RGO, **b** ZnO, **c** ZnO:B and **d** RGO/ZnO:B nanoparticles

at 160 °C. The characteristic diffraction peak of GO at 11.24° (Fig. 2b) disappeared upon heat treatment, and the GO was reduced to RGO (Fig. 4a). XRD patterns of the ZnO particles obtained at pH 9 are shown in Fig. 4b. The diffraction patterns of the obtained ZnO particles were $2\theta = 31.7°$, 34.4°, 36.2°, 47.4°, 56.5°, 62.7°, 66.8°, 67.9° and 69.1°. The planes corresponding to these angle values are determined to be (100), (002), (101), (102), (110), (103), (200), (112), and (201). The planes corresponding to these angle values show that the particles obtained are of the ZnO phase with a hexagonal wurtzite structure (PDF-2, reference code: 01–079-2205). Figure 4c shows the XRD pattern of the ZnO:B particles containing 5% by weight of boron. The XRD spectrum of the obtained ZnO:B particles did not show any peaks associated with boron or other boron compounds. This can be explained by the fact that boron atoms are replaced by Zn atoms and enter the ZnO structure. In addition, with the addition of boron, the intensity of the (001) peak decreased. This indicates a decrease in the quality of the crystal. This can be explained by the fact that boron atoms enter the ZnO structure by replacing them with Zn atoms, and the number of Zn atoms decreases as a

function of the peak density [35]. The XRD pattern of the RGO/ZnO:B composite particle is shown in Fig. 4d. As seen from the XRD spectrum, the RGO/ZnO:B structure consists of a mixture of the wurtzite ZnO phase (PDF-2, reference code: 01–079-2205) and the zinc hydroxide phase called simoncolleite ($Zn_5(OH)_8Cl_2$). H_2O) (PDF2: reference code: 00–076-0922). As shown in Fig. 4d, the peaks corresponding to zinc oxide and zinc hydroxide are clearly visible. However, no peaks corresponding to RGO were found. This can probably be explained by the aggregation of ZnO:B particles on the graphene layers. The reason for the formation of a hydroxide structure in the composite particle is that the ZnO:B structure, which is placed in the GO solution used in the preparation of the composite material by the hydrothermal method, undergoes rehydration and is transformed into a simoncolleite structure.

Figure 5 shows SEM images of the (a) RGO, (b) ZnO, (c) ZnO:B, and (d) RGO/ZnO:B nanoparticles. The layers of reduced graphene oxide (RGO) (Fig. 5a) are clustered together, so they adhere to each other. This is a typical result for hydrothermally fabricated reduced graphene oxide. By examining the SEM images (Fig. 5b) of the ZnO particles (pH 9), it can be observed that they are formed in the form of hexagonal rods with dimensions of approximately 500 nm. The particle size of the ZnO particles obtained by the hydrothermal method decreases at high pH values, as shown by many studies in the literature [36, 37]. In addition, high pH values have been shown to increase antimicrobial activity in studies in the literature [38]. Figure 5c shows an SEM image of the ZnO:B particles with a boron content of 5% by weight. The morphological structure was found to be a hexagonal rod and was approximately 100 nm in size according to the SEM image (Fig. 5c). SEM images show that the doping of boron results in a reduction in particle size. SEM images of the RGO/ZnO:B nanocomposite particles are shown in Fig. 5d. Hexagonal rod-like ZnO:B particles are observed to be distributed among the RGO layers in the SEM images. The crystal structure of the hexagonal bar-shaped ZnO:B particles under the RGO sheets shows a wurtzite structure. ZnO:B particles are thought to bond to the remaining oxygen atoms between the graphene oxide layers in this distribution.

3.2 Antimicrobial Activity

The antimicrobial activities of the RGO, ZnO, ZnO:B and RGO/ZnO:Br NPs synthesized in this study were evaluated against different reference bacterial strains. The obtained results demonstrated that the synthesized NPs generally exhibited an antimicrobial effect against the tested pathogenic bacteria (Table 1).

The investigated ZnO and ZnO:B NPs showed strong antimicrobial activity against the clinically important *E. coli*, *P. aeruginosa* and *B. cereus strains*. The RGO NPs did not have any inhibitory effect on the test strains (Fig. 6). Interestingly, RGO was also found to have a negative effect on the antimicrobial activity of the ZnO:B nanocomposite. Notably, the RGO/ZnO:B nanocomposite had low MIC values for the tested microorganisms. A comparison of the results obtained for the NPs with those obtained for gentamicin, which was

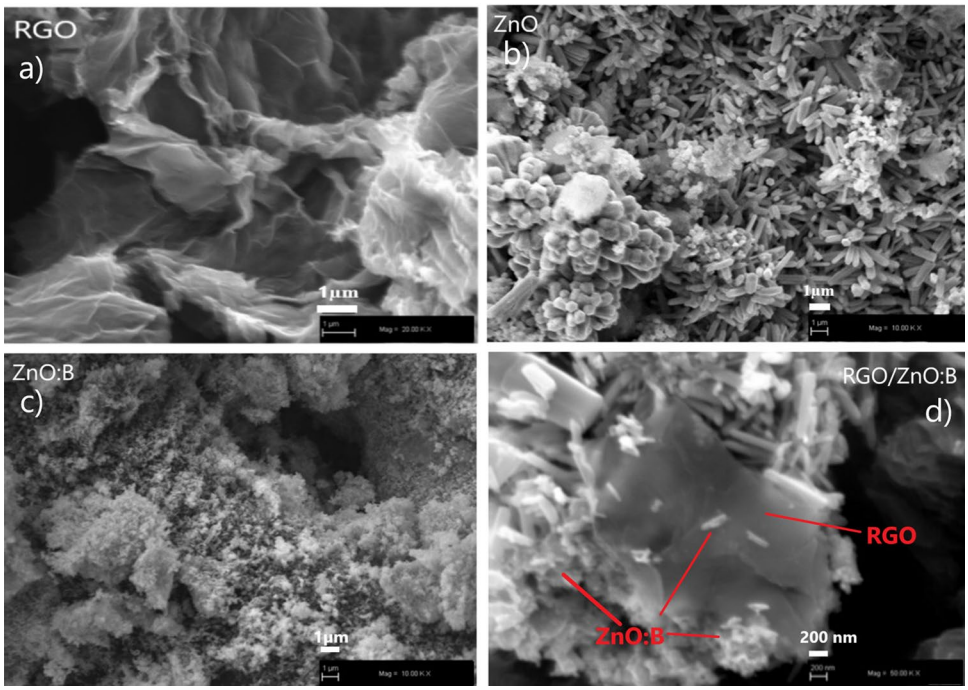

Fig. 5 SEM images of **a** RGO, **b** ZnO, **c** ZnO:B and **d** RGO/ZnO:B nanoparticles

Table 1 Antimicrobial zone diameters of the synthesized nanoparticles on pathogenic type strains

NPs	Antimicrobial zone diameter					
	E. coli 25,922	*P. aeruginosa* 27,853	*S. aureus* 25,923	*E. faecalis* ATCC 29212	*S. epidermidis* ATCC 12228	*B. cereus* 14,579
RGO	ND	11 ± 0.6	10 ± 1.2	22 ± 0.3	ND	ND
ZnO	21 ± 1.3	18 ± 0.3	21 ± 0.7	23 ± 0.7	24 ± 0.9	40 ± 0.8
ZnO:B	22 ± 1.4	20 ± 0.8	16 ± 0.8	26 ± 1.5	25 ± 12	35 ± 1.2
RGO/ZnO:B	ND	12 ± 1.2	11 ± 0.5	12 ± 0.4	ND	13 ± 0.4
MIC[a] (uM)						
RGO	ND	128	128	32	ND	ND
ZnO	16	32	64	16	16	0.5
ZnO:B	8	16	16	8	4	0.5
RGO/ZnO:B	ND	8	16	8	ND	4
CN[b]	0.5	1	0.5	1	1	0.5

[a]The minimum inhibitory concentration (MIC) was determined as the lowest concentration inhibiting bacterial growth determined in three independent experiments performed in triplicate

[b]CN: Gentemycin

used as a positive control in the present study showed that the MIC values were close to each other.

3.3 Antibiofilm Activity

In our study, the antibiofilm activity of the synthesized nanoparticles was determined using *E. coli* ATCC 25922 (Fig. 7) and *P. aeruginosa* ATCC 27853 strains (Fig. 8). As a result of the study, biofilm inhibition by the ZnO:B nanocomposites was greater for both strains. At a concentration of 20 mg/mL, the ZnO:B nanocomposite had 42.13% biofilm inhibition of *E. coli* and 36.21% biofilm inhibition of *P. aeruginosa*, while the RGO/ZnO:B nanocomposite had a specific inhibitory effect on 34.25% and 30.16% of the *E. coli* strains, respectively. The antibiofilm effect of the tested nanocompounds was greater on *E. coli* than on *P. aeruginosa*. Due to their strong antibacterial and antibiofilm activities, ZnO:B NPs are considered to be potential candidates for both biomedical and industrial applications.

Considering that antibiotic resistance is a major public health problem, it has become essential to develop new treatment agents and treatment strategies. For this purpose, in our study, RGO and boron-containing ZnO nanocomposites based on ZnO NPs were synthesized, and their effectiveness was evaluated for biological applications. The obtained

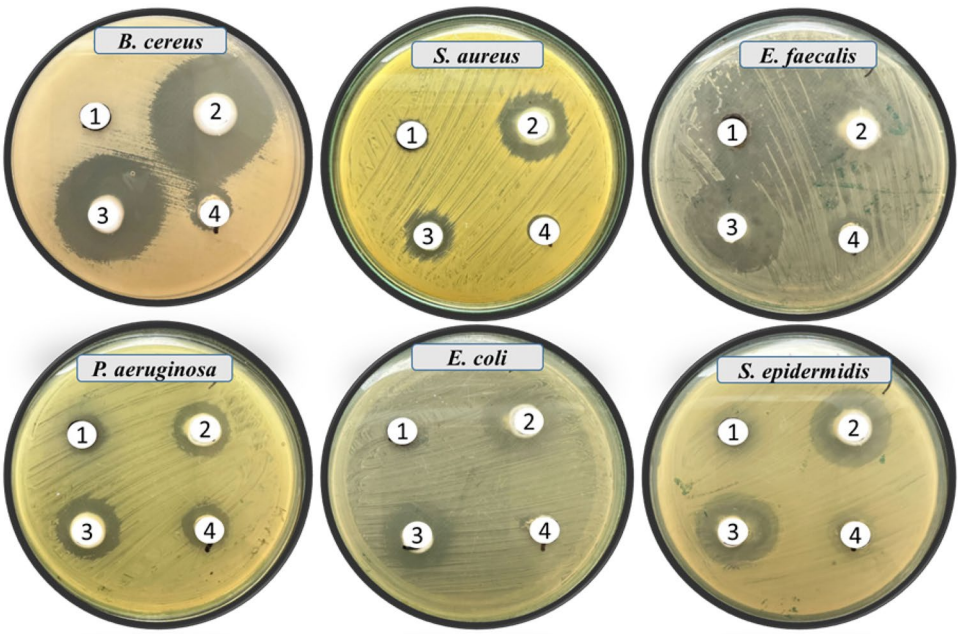

Fig. 6 Inhibition zone activities of NP on tested pathogenic strains. 1: RGO, 2: ZnO, 3: ZnO:B, 4: RGO/ZnO:B

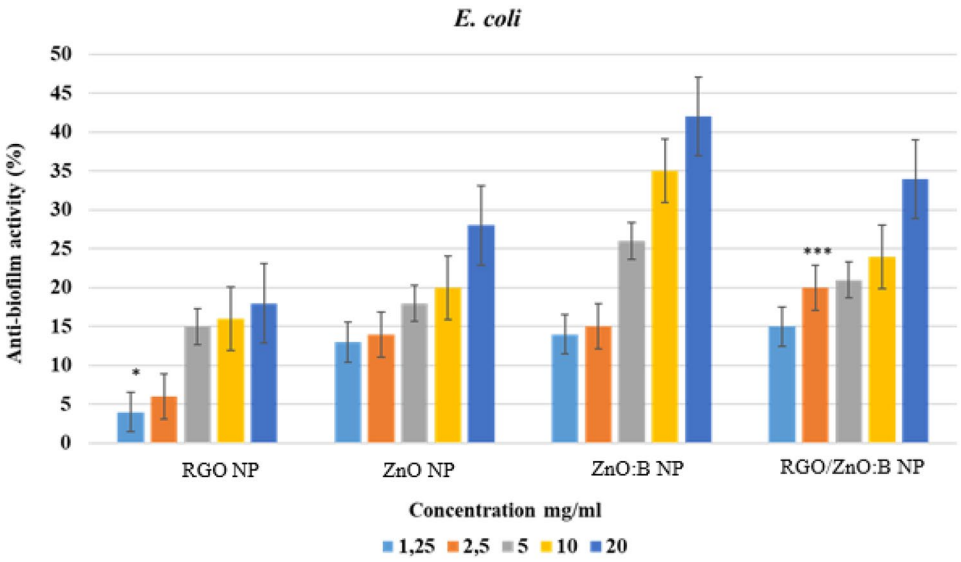

Fig. 7 Antibiofilm activity of different concentrations of nanoparticles on the *E. coli* ATCC 25922 type strain. The statistical significance values ***, **, and * denote significance at $p < 0.0001$, $p < 0.01$, and $p < 0.05$, respectively—whereas ns denotes nonsignificance

results demonstrated that the RGO and RGO/ZnO:B nanoparticles had very little inhibitory activity, while the ZnO and ZnO:B nanoparticles had a significant effect on the tested pathogenic microorganisms. RGO is known to have an antimicrobial effect and even a synergistic effect when produced as a nanocomposite [12, 39, 40]. In our study, however, no such effect was observed against pathogenic microorganisms. This difference is thought to be due to the structure and concentration of the compounds used to synthesize the nanocomposites, the type of bacteria (different cell wall structures and mechanism of action) and the effect of time. For example, one study investigated the antimicrobial activity of RGO, RGO/Cu and RGO/Ag nanocomposites. The effect of the synthesized nanocomposites was tested based on the viability rate of *E. coli* and *S. aureus* bacteria over different time periods (0 h- 3 h- 24 h). The results showed that RGO had no microbicidal effect on the test microorganisms, while the nanocomposites had an inhibitory effect over time. The bactericidal use of RGO is limited due to the stacking of graphene sheets by van der Waals forces [41]. Although graphene nanomaterials have excellent surface properties, they have strong interplanar interactions that limit their antibacterial activity and make them insoluble due to particle aggregation [42]. ZnO NPs are now known to be powerful antimicrobial agents [43–46]. These strains exhibited positive antimicrobial and antibiofilm properties in our study. Gram-negative and gram-positive bacteria can lose their viability due to the broad-spectrum antibacterial effect of nanoparticles. Physical contact between nanoparticles and microorganisms is the most important factor influencing

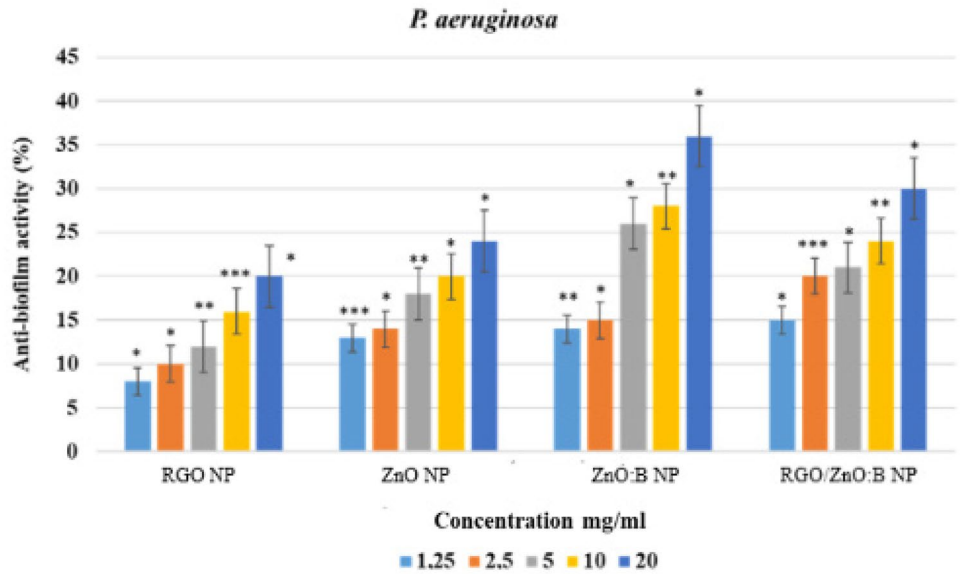

Fig. 8 Antibiofilm activity of different concentrations of nanoparticles on the *P. aeruginosa* ATCC 27853 type strain. The statistical significance values ***, **, and * denote significance at $p < 0.0001$, $p < 0.01$, and $p < 0.05$—whereas ns

this process. NPs adhering to the surface of microorganisms cause charge transfer and oxidative stress via electrochemical events such as electrostatic attraction, van der Waals forces and hydrophobic interactions [41]. Metal oxide NPs can alter the morphology of microorganisms and the formation of biofilms, reduce the permeability of microbial membranes and cause oxidative stress on genes through the formation of H_2O_2 [12]. These events cause cell death. The difference in cell wall structure between gram-negative and gram-positive bacteria is another parameter that affects bactericidal activity. In gram-positive bacteria, the cell wall contains a peptodoglycan layer, which causes the cell wall to be thicker and thus reduces the permeability of the cell membrane. This is a limitation to the intracellular release of NPs.

However, compared with the other NPs, the boron-supplemented ZnO NPs synthesized in our study were the most effective biological inhibitors and produced a synergistic effect. Boron-containing bioactive molecules are considered potential drug candidates and exhibit important biological activities, such as anti-inflammatory, antifungal and antibacterial effects [47–49]. When the intracellular molecular mechanism is examined, it is thought that boron binds to enzymes and subsequently interacts with target proteins, leading to reversible inhibition and thus exerting an inhibitory effect [50]. Boron compounds have been reported to have beneficial healing properties and thus great potential in the wound healing process [51]. The antibacterial properties of the synthesized AgNPs, CuNPs, AgCuNPs and AgCu:B NPs were investigated against *S. aureus,* and it was found that AgCu:B NPs exhibited a stronger bactericidal effect than the other NPs [16]. Furthermore, AgB NPs showed stronger antimicrobial and antibiofilm properties against urinary tract pathogens than boric acid and AgNPs [52]. In another study, bimetallic boron oxide–zinc oxide nanoparticles (B_2O_3–ZnO NPs) were synthesized, and these NPs were examined for their anticancer, antimicrobial and antioxidant activities. B_2O_3–ZnO NPs exhibited promising antibacterial activity against *E. coli*, *P. aeruginosa*, *B. subtilis* and *S. aureus* [19]. Furthermore, the antimicrobial properties of boron-doped TiO_2 NPs synthesized at different rates using a microwave-assisted solvothermic method were analyzed against *S. aureus* and *E. coli*. As the amount of added boron increased, the TiO_2 NPs caused an increase in the inhibition zones of *S. aureus* and *E. coli* [53]. The antibacterial properties of the synthesized AgNPs, CuNPs, AgCuNPs and AgCu:B NPs were investigated against *S. aureus* bacteria, and it was found that AgCu:B NPs exhibited a stronger bactericidal effect than the other NPs [16]. Furthermore, AgB NPs showed stronger antimicrobial and antibiofilm properties against urinary tract pathogens than boric acid and AgNPs [52]. The addition of boron to nanoparticles has been shown to increase the biological efficacy of the material, similar to the findings of this study.

4 Conclusion

Consequently, the antimicrobial and antibiofilm effects of the produced RGO and RGO-based nanocomposites were not found to be significant, which was thought to be due to the type of bacteria, concentration of NPs and time periods. However, the synthesized boron-reinforced ZnO nanocomposite showed a strong biological effect. There are very few studies on the antimicrobial and antibiofilm properties of ZnO NPs reinforced with boron. The results of this study are promising and can serve as a reference for future studies. In particular, it has significant potential as a new antibacterial drug candidate and as a new treatment regimen to overcome major public health problems, such as antibiotic resistance.

Declarations

Researcher Contribution Rate Statement Summary The authors declare that they have contributed equally to the article.

Conflict of Interest Statement The authors declare that they have no conflicts of interest.

References

1. M.K.Y. Soliman, S.S. Salem, M. Abu-Elghait, M.S. Azab, Biosynthesis of Silver and Gold Nanoparticles and Their Efficacy Towards Antibacterial, Antibiofilm, Cytotoxicity, and Antioxidant Activities. Appl. Biochem. Biotechnol. **195**(2), 1158–1183 (2023). https://doi.org/10.1007/s12010-022-04199-7
2. N. Jubair, M. Rajagopal, S. Chinnappan, N.B. Abdullah, A. Fatima, Review on the Antibacterial Mechanism of Plant-Derived Compounds against Multidrug-Resistant Bacteria (MDR). Evidence-based Complement. Altern. Med. 2021 (2021). https://doi.org/10.1155/2021/3663315
3. P. Singh, S. Pandit, C. Jers, A.S. Joshi, J. Garnæs, I. Mijakovic, Silver nanoparticles produced from Cedecea sp. exhibit antibiofilm activity and remarkable stability. Sci. Rep. **11**(1), 1–13 (2021). https://doi.org/10.1038/s41598-021-92006-4
4. M.G. Kang, F. Khan, D.M. Jo, D.K. Oh, N. Tabassum, Y.M. Kim, Antibiofilm and Antivirulence Activities of Gold and Zinc Oxide Nanoparticles Synthesized from Kimchi-Isolated Leuconostoc sp. Strain C2. Antibiotics. **11**(11) (2022). https://doi.org/10.3390/antibiotics11111524
5. E. Sánchez-López et al., Metal-based nanoparticles as antimicrobial agents: An overview. Nanomaterials **10**(2), 1–39 (2020). https://doi.org/10.3390/nano10020292
6. G.T. Anand, R. Nithiyavathi, R. Ramesh, S. John Sundaram, K. Kaviyarasu, Structural and optical properties of nickel oxide nanoparticles: Investigation of antimicrobial applications. Surf Interfaces. **18**(2019), 100460 (2020). https://doi.org/10.1016/j.surfin.2020.100460
7. P.P. Mahamuni et al., Synthesis and characterization of zinc oxide nanoparticles by using polyol chemistry for their antimicrobial and antibiofilm activity. Biochem. Biophys. Rep. **17**(2018), 71–80 (2019). https://doi.org/10.1016/j.bbrep.2018.11.007
8. S.A. Khan, S. Shahid, A. Ayaz, J. Alkahtani, M.S. Elshikh, T. Riaz, Phytomolecules-coated NiO nanoparticles synthesis using

abutilon indicum leaf extract: Antioxidant, antibacterial, and anticancer activities. Int. J. Nanomedicine **16**, 1757–1773 (2021). https://doi.org/10.2147/IJN.S294012
9. V. Tsikourkitoudi, B. Henriques-Normark, G.A. Sotiriou, Inorganic nanoparticle engineering against bacterial infections. Curr. Opin. Chem. Eng. **38**, 100872 (2022). https://doi.org/10.1016/j.coche.2022.100872
10. Q. Liang, F. Qiao, X. Cui, X. Hou, Controlling the morphology of ZnO structures via low temperature hydrothermal method and their optoelectronic application. Mater. Sci. Semicond. Process. **89**(2018), 154–160 (2019). https://doi.org/10.1016/j.mssp.2018.09.007
11. S. Mohan, M. Vellakkat, A. Aravind, U. Reka, Hydrothermal synthesis and characterization of Zinc Oxide nanoparticles of various shapes under different reaction conditions. Nano Express **1**(3), 30028 (2020). https://doi.org/10.1088/2632-959X/abc813
12. S. Elbasuney, G.S. El-Sayyad, H. Tantawy, A.H. Hashem, Promising antimicrobial and antibiofilm activities of reduced graphene oxide-metal oxide (RGO-NiO, RGO-AgO, and RGO-ZnO) nanocomposites. RSC Adv. **11**(42), 25961–25975 (2021). https://doi.org/10.1039/d1ra04542c
13. M.I. Khan et al., Investigation of in vitro antibacterial and seed germination properties of green synthesized pure and nickel doped ZnO nanoparticles. Phys. B Condens. Matter **601**(2020), 412563 (2021). https://doi.org/10.1016/j.physb.2020.412563
14. A.M. Shehabeldine et al., Potential Antimicrobial and Antibiofilm Properties of Copper Oxide Nanoparticles: Time-Kill Kinetic Essay and Ultrastructure of Pathogenic Bacterial Cells. Appl. Biochem. Biotechnol. **195**(1), 467–485 (2023). https://doi.org/10.1007/s12010-022-04120-2
15. Y. Wang, X. Wang, L. Li, Y. Wu, Q. Yu, An experimental and theoretical study on the photocatalytic antibacterial activity of boron-doped TiO2 nanoparticles. Ceram. Int. **48**(1), 604–614 (2022). https://doi.org/10.1016/j.ceramint.2021.09.139
16. T. Abdulrehman et al., Boron doped silver-copper alloy nanoparticle targeting intracellular S. Aureus in bone cells. PLoS ONE **15**(4), 1–18 (2020). https://doi.org/10.1371/journal.pone.0231276
17. S. Archana et al., Synthesis of nickel oxide grafted graphene oxide nanocomposites - A systematic research on chemisorption of heavy metal ions and its antibacterial activity. Environ. Nanotechnology, Monit. Manag. **16**(May), 100486 (2021). https://doi.org/10.1016/j.enmm.2021.100486
18. J. Xu et al., Antibiofilm Effect of Cinnamaldehyde-Chitosan Nanoparticles against the Biofilm of *Staphylococcus aureus*. Antibiotics **11**(10), 1–13 (2022). https://doi.org/10.3390/antibiotics11101403
19. A.H. Hashem, S.H. Rizk, M.A. Abdel-Maksoud, W.H. Al-Qahtani, H. AbdElgawad, G.S. El-Sayyad, Unveiling anticancer, antimicrobial, and antioxidant activities of novel synthesized bimetallic boron oxide-zinc oxide nanoparticles. RSC Adv. **13**(30), 20856–20867 (2023). https://doi.org/10.1039/d3ra03413e
20. R. Kucukosman et al., Boron-based magnesium diboride nanosheets preparation and tested for antimicrobial properties for PES membrane. Chemosphere **339** (2023). https://doi.org/10.1016/j.chemosphere.2023.139340
21. M. Umar et al., Designing of Te-doped ZnO and S-g-C3N4/Te-ZnO nanocomposites as excellent photocatalytic and antimicrobial agents. Polyhedron **245**(May), 116664 (2023). https://doi.org/10.1016/j.poly.2023.116664
22. J.G. Cuadra et al., ZnO/Ag Nanocomposites with Enhanced Antimicrobial Activity. Appl. Sci. **12**(10), 1–13 (2022). https://doi.org/10.3390/app12105023
23. R. Ahmadi, R. Fattahi Nafchi, P. Sangpour, M. Bagheri, E. Badiei, A comparative study: Green synthesis and evaluation of ZnO-GO and ZnO-RGO nanocomposites for antibacterial applications. Mater. Sci. Eng. B **294**(2022), 116555 (2023). https://doi.org/10.1016/j.mseb.2023.116555
24. A. Al Baroot, M. Alheshibri, Q.A. Drmosh, S. Akhtar, E. Kotb, K.A. Elsayed, A novel approach for fabrication ZnO/CuO nanocomposite via laser ablation in liquid and its antibacterial activity: A novel approach for fabrication ZnO/CuO nanocomposite, Arab. J. Chem. **15**(2), . 103606 (2022). https://doi.org/10.1016/j.arabjc.2021.103606
25. A.A. Menazea, N.S. Awwad, Antibacterial activity of TiO2 doped ZnO composite synthesized via laser ablation route for antimicrobial application. J. Mater. Res. Technol. **9**(4), 9434–9441 (2020). https://doi.org/10.1016/j.jmrt.2020.05.103
26. E. Kiray, Antibiofilm and Anti-Quorum Sensing Activities of Vaginal Origin Probiotics. Eur. J. Biol. **80**(2), 82–90 (2021). https://doi.org/10.26650/EurJBiol.2021.932640
27. B. Kowalska-Krochmal, R. Dudek-Wicher, The minimum inhibitory concentration of antibiotics: Methods, interpretation, clinical relevance. Pathogens **10**(2), 1–21 (2021). https://doi.org/10.3390/pathogens10020165
28. N.A. Theodora, V. Dominika, D.E. Waturangi, Screening and quantification of anti-quorum sensing and antibiofilm activities of phyllosphere bacteria against biofilm forming bacteria. BMC. Res. Notes **12**(1), 10–14 (2019). https://doi.org/10.1186/s13104-019-4775-1
29. V. Gupta, N. Sharma, U. Singh, M. Arif, A. Singh, Higher oxidation level in graphene oxide. Optik (Stuttg) **143**, 115–124 (2017). https://doi.org/10.1016/j.ijleo.2017.05.100
30. J. Guerrero-Contreras, F. Caballero-Briones, Graphene oxide powders with different oxidation degree, prepared by synthesis variations of the Hummers method. Mater. Chem. Phys. **153**, 209–220 (2015). https://doi.org/10.1016/j.matchemphys.2015.01.005
31. R.M. Nauman Javed, A. Al-Othman, M. Tawalbeh, A.G. Olabi, Recent developments in graphene and graphene oxide materials for polymer electrolyte membrane fuel cells applications. Renew. Sustain. Energy Rev. **168**(January), 112836 (2022). https://doi.org/10.1016/j.rser.2022.112836
32. V. Sharma, Y. Jain, M. Kumari, R. Gupta, S.K. Sharma, K. Sachdev, Synthesis and Characterization of Graphene Oxide (GO) and Reduced Graphene Oxide (rGO) for Gas Sensing Application. Macromol. Symp. **376**(1), 1–5 (2017). https://doi.org/10.1002/masy.201700006
33. R. Al-Gaashani, A. Najjar, Y. Zakaria, S. Mansour, M.A. Atieh, XPS and structural studies of high quality graphene oxide and reduced graphene oxide prepared by different chemical oxidation methods. Ceram. Int. **45**(11), 14439–14448 (2019). https://doi.org/10.1016/j.ceramint.2019.04.165
34. M. Muniyalakshmi, K. Sethuraman, D. Silambarasan, Synthesis and characterization of graphene oxide nanosheets. Mater. Today, Proc. **21**, 408–410 (2020). https://doi.org/10.1016/j.matpr.2019.06.375
35. T. Hurma, Effect of boron doping concentration on structural optical electrical properties of nanostructured ZnO films. J. Mol. Struct. **1189**, 1–7 (2019). https://doi.org/10.1016/j.molstruc.2019.03.096
36. M.J. Chithra, M. Sathya, K. Pushpanathan, Effect of pH on crystal size and photoluminescence property of zno nanoparticles prepared by chemical precipitation method. Acta Metall. Sin. English Lett. **28**(3), 394–404 (2015). https://doi.org/10.1007/s40195-015-0218-8
37. N. Kumaresan, K. Ramamurthi, R. Ramesh Babu, K. Sethuraman, S. Moorthy Babu, Hydrothermally grown ZnO nanoparticles for effective photocatalytic activity. Appl. Surf. Sci. **418**, 138–146 (2017). https://doi.org/10.1016/j.apsusc.2016.12.231
38. S.B. Ghaffari, M.H. Sarrafzadeh, M. Salami, M.R. Khorramizadeh, A pH-sensitive delivery system based on N-succinyl chitosan-ZnO nanoparticles for improving antibacterial and anticancer activities of curcumin. Int. J. Biol. Macromol. **151**, 428–440 (2020). https://doi.org/10.1016/j.ijbiomac.2020.02.141
39. R. Niranjan, S. Zafar, B. Lochab, R. Priyadarshini, Synthesis and Characterization of Sulfur and Sulfur-Selenium Nanoparticles

Loaded on Reduced Graphene Oxide and Their Antibacterial Activity against Gram-Positive Pathogens. Nanomaterials **12**(2) (2022). https://doi.org/10.3390/nano12020191
40. O. Usman et al., Enhanced Bactericidal Action of rGO-ZnO Hybrids Prepared by the One-Pot Coprecipitation Approach. ACS Omega **7**(30), 26715–26722 (2022). https://doi.org/10.1021/acsomega.2c03049
41. D. Kichukova, I. Spassova, A. Kostadinova, A. Staneva, D. Kovacheva, Facile Synthesized Cu–RGO and Ag–RGO Nanocomposites with Potential Biomedical Applications. Nanomaterials **12**(12) (2022). https://doi.org/10.3390/nano12122096
42. V. Ahmad, M.O. Ansari, Synthesis, Characterization, and Evaluation of Antimicrobial Efficacy of Reduced Graphene–ZnO–Copper Nanocomplex. Antibiotics **12**(2) (2023). https://doi.org/10.3390/antibiotics12020246
43. M.J. Klink, N. Laloo, A.L. Taka, V.E. Pakade, E. Monapathi, J.S. Modise, Synthesis , Characterization and Antimicrobial Activity of Zinc Yeast Pathogens. (2022)
44. D.V. Francis, M.N. Jayakumar, H. Ahmad, T. Gokhale, Antimicrobial Activity of Biogenic Metal Oxide Nanoparticles and Their Synergistic Effect on Clinical Pathogens. Int. J. Mol. Sci. **24**(12) (2023). https://doi.org/10.3390/ijms24129998
45. W.M. Abdelraheem, E.S. Mohamed, The effect of Zinc Oxide nanoparticles on *Pseudomonas aeruginosa* biofilm formation and virulence genes expression. J. Infect. Dev. Ctries. **15**(6), 826–832 (2021). https://doi.org/10.3855/jidc.13958
46. W.M. Abdelraheem, R.M.M. Khairy, A.I. Zaki, S.H. Zaki, Effect of ZnO nanoparticles on methicillin, vancomycin, linezolid resistance and biofilm formation in *Staphylococcus aureus* isolates. Ann. Clin. Microbiol. Antimicrob. **20**(1), 1–11 (2021). https://doi.org/10.1186/s12941-021-00459-2
47. Y. Zheng, X.K. Li, Y. Wang, L. Cai, The role of zinc, copper and iron in the pathogenesis of diabetes and diabetic complications: Therapeutic effects by chelators. Hemoglobin **32**(1–2), 135–145 (2008)
48. H. Yang et al., Synthesis of boron carbonitride nanosheets using for delivering paclitaxel and their antitumor activity. Colloids Surf. B Biointerfaces **198**(2020), 111479 (2021). https://doi.org/10.1016/j.colsurfb.2020.111479
49. F. Yang, M. Zhu, J. Zhang, H. Zhou, Synthesis of biologically active boron-containing compounds. Medchemcomm **9**(2), 201–211 (2018). https://doi.org/10.1039/c7md00552k
50. Y. Zhu, P. Prommana, N.S. Hosmane, P. Coghi, C. Uthaipibull, Y. Zhang, Functionalized Boron Nanoparticles as Potential Promising Antimalarial Agents. ACS Omega **7**(7), 5864–5869 (2022). https://doi.org/10.1021/acsomega.1c05888
51. H. Türkez et al., Lipoic Acid Conjugated Boron Hybrids Enhance Wound Healing and Antimicrobial Processes. Pharmaceutics **15**(1) (2023). https://doi.org/10.3390/pharmaceutics15010149
52. A.I. El-Batal, G.S. El-Sayyad, N.E. Al-Hazmi, M. Gobara, Antibiofilm and Antimicrobial Activities of Silver Boron Nanoparticles Synthesized by PVP Polymer and Gamma Rays Against Urinary Tract Pathogens. J. Clust. Sci. **30**(4), 947–964 (2019). https://doi.org/10.1007/s10876-019-01553-4
53. N.F. Andrade Neto, P. Zanatta, L.E. Nascimento, R.M. Nascimento, M.R.D. Bomio, F.V. Motta, Characterization and Photoluminescent, Photocatalytic and Antimicrobial Properties of Boron-Doped TiO 2 Nanoparticles Obtained by Microwave-Assisted Solvothermic Method. J. Electron. Mater. **48**(5), 3145–3156 (2019). https://doi.org/10.1007/s11664-019-07076-y